FINAL PUBLISHABLE REPORT

Grant Agreement number	18SIB07
Project short name	GIQS
Project full title	Graphene Impedance Quantum Standard

Project start date and duration:		1 June 2019, 36 months
Coordinator: Klaus Pierz, PTB	Tel: +49 531 592 2412	E-mail: klaus.pierz@ptb.de
Project website address: https://www.ptb.de/empir2019/giqs/home/		
Internal Funded Partners: 1. PTB, Germany 2. CMI, Czech Republic 3. INRIM, Italy 4. LNE, France 5. METAS, Switzerland 6. RISE, Sweden 7. VTT, Finland	External Funded Partners: 8. CNRS, France 9. NIMT, Thailand 10. POLITO, Italy	Unfunded Partners: 11. KRISS, Korea, Republic of
RMG1: INRIM, Italy (Employing organisation); PTB, Germany (Guestworking organisation)		

TABLE OF CONTENTS

1 Overview

The aim of this project was to enable an economically efficient traceability of impedance quantities to the defining constants of the revised International System of Units (SI). This will simplify the calibration support which European and other National Metrology Institutes (NMIs) provide to the electronics industries. To meet these goals the partners have successfully developed high-quality graphene-based QHE impedance standards and improved the performance and the working range of digital- and Josephson-impedance bridges. These pieces of equipment are easier to operate and the provided Good Practice Guide will allow the users a simpler traceability of the impedance units to the quantum Hall effect with high metrological accuracy. The developed cryogenic system components for operating the quantum devices will help to simplify the challenging requirements of impedance measurements in the future.

2 Need

Electronic components rely, for their international competitiveness, on the application of mutually agreed measurements during their production and use. Electrical impedance (capacitance, inductance) is a quantity in this field that is practically of equal importance to voltage and resistance. It is more important than current, as the sensors, which are used in numerous contexts either rely on resistance or, more often, on contactless capacitive methods. For voltage and resistance, the “gold standards” of traceability, namely the Josephson effect (JE) and the quantum Hall effect (QHE), have been used in major NMIs for a long time. Impedance standards on the other hand still require many calibration steps with complicated measurement setups to trace them to the QHE.

At present, only a very few quantum standards are in use outside of the NMIs due to the high investment, high operational costs, and complexity of use. The quantum traceability of the impedance unit, the farad, would clearly benefit if an economically viable route was established. However, the complex calibration chains from the QHE to different capacitance and inductance values only exist in some of the largest NMIs. This was not acceptable and a shorter and simpler traceability chain of impedance to quantum standards, which is available and affordable for all NMIs, calibration centres and industries (e.g., automotive and mobile electronics), was clearly needed.

At this point, the need to utilise graphene came into play: its potential for metrology was understood almost immediately, because in graphene the QHE can exist at much lower magnetic fields (below 6 T) and at higher temperatures (above 4 K) than in conventional systems. The fundamental constant realisation for the DC QHE has been simplified by using graphene. The realisation of the corresponding fundamental constant for the AC units of impedance, i.e. capacitance and inductance, has also benefited from graphene with its much less demanding operational margins with respect to temperature and magnetic field. In addition, simpler and more flexible AC instrumentation had to be further developed, optimised and adapted for the use of graphene devices that are directly operated in the AC regime, thus avoiding a troublesome DC resistance to AC impedance transfer procedure.

3 Objectives

The overall objective was to combine novel digital impedance measurement bridges with the QHE material graphene in a simplified cryogenic environment. This has provided European NMIs, calibration centres and industry with the technology that is needed to enable the practical realisation of electrical impedance units (ohm, farad, henry) in the revised SI.

The specific objectives of the project were:

1. To optimise and to tailor graphene material and graphene devices in order to improve the understanding of the graphene AC quantised Hall effect (AC-QHE), as the basis for the traceability of impedance units to the QHE at temperatures of 4 K or higher in magnetic fields that are as low as possible - at most 6 T.
2. To advance digital bridges for the capacitance range from 10 pF to 10 nF at frequencies up to 100 kHz, and to develop an impedance bridge working with spectrally pure Josephson voltages up to 50 kHz in the entire complex plane.

3. To combine graphene devices with a Josephson impedance bridge (with a target uncertainty below 0.01 μΩ/Ω), and with a full digital bridge for simplified operation, (with a target uncertainty in the 0.1 μΩ/Ω range), in order to provide traceability for capacitance to the QHE.
4. To develop and investigate a cryo-cooler system hosting the superconducting Josephson device and the graphene device, both operating at AC and serving as the core element of a quantum resistance and impedance standard in the revised SI.
5. To facilitate the take up of the technology and measurement infrastructure developed in the project by the measurement supply chain (e.g. graphene manufacturers), standards developing organisations and end users (e.g. NMIs and calibration centres as well as the European Commission's Graphene Flagship).

4 Results

4.1 Optimisation and tailoring graphene material and graphene devices for the AC Quantum Hall effect (Objective 1)

Introduction

The first objective of the GIQS project was to optimise graphene devices for the DC and AC QHE at higher temperatures and reduced magnetic fields. This has been achieved by optimising every step of device fabrication, i.e. the graphene growth methods on SiC, the processing of large Hall bars, and finally the tuning of charge carrier density in graphene through chemical treatments. The devices have been tested extensively both as a support to device optimisation and in order to improve the understanding of the DC and AC QHE in graphene as the basis for the traceability of impedance units to the QHE at temperatures of 4 K or higher and in magnetic fields that are as low as possible - at most 6 T.

4.1.1 Graphene growth

Three methods have been used in the GIQS project to grow graphene on SiC: the “classic” silicon-sublimation at KRISS, the polymer assisted Si-sublimation at PTB, and the CVD in hydrogen atmosphere at CNRS.

The silicon-sublimation (Si-sublimation) method allows us to grow graphene on SiC at a high temperature by sublimating silicon atoms from the SiC surface. The control of Si sublimation is essential to obtain a metrology-grade SiC graphene with a low step height and a high monolayer coverage. For instance, it is well known that slow Si sublimation prevents step bunching for graphene growth. KRISS has modified its graphite susceptor by reducing the gap size to about 50 µm for a slow Si sublimation. SiC graphene grown in the modified graphite susceptor shows a low step height below 1.5 nm and monolayer coverage above 95 %, indicating high-quality graphene on SiC.

The Polymer-Assisted Sublimation Growth (PASG) methods differ from Si-sublimation by the deposition on SiC, before annealing, of a polymer film which serves as an extra carbon source and allows the SiC surface to be stabilised by enhanced formation of uniformly distributed buffer layer domains. PTB has further improved PASG and determined optimised polymer deposition and annealing parameters to grow graphene for DC and AC-QHE. Using optimal polymer deposition, the graphene films present a full monolayer coverage without buffer layer or bilayer patches, as attested by confocal microscopy (Figure 4.1(a)), atomic force microscopy (AFM) and scanning electron microscopy (SEM). AFM also evidences the absence of step bunching (Figure 4.1(b)). Finally, the quality and the uniformity of the film are attested by Raman cartography (Figure 4.1(c)).

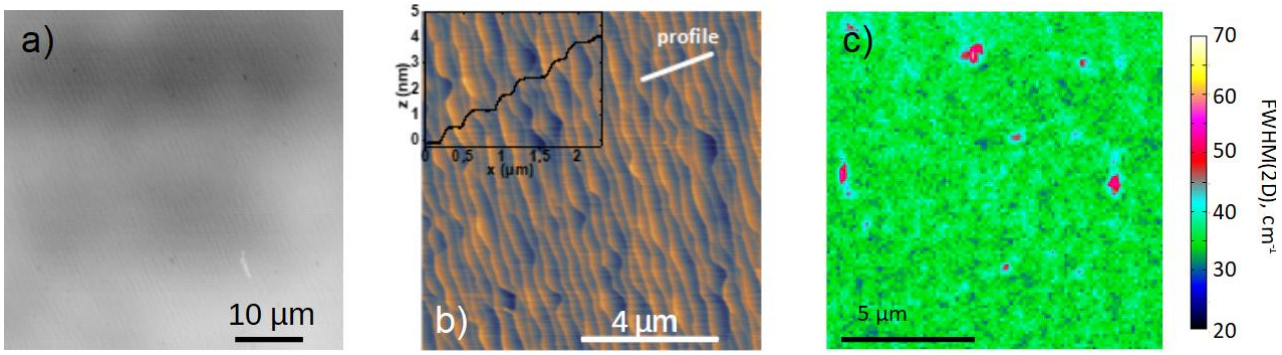

Figure 4.1.1: *Optical microscopy (a), atomic force microscopy (b) and Raman spectroscopy mapping (c) on samples obtained by polymer assisted sublimation growth (PASG)*

The CVD growth of graphene on SiC in a hydrogen atmosphere strongly differs from Si-sublimation growth by the hydrogen atmosphere which prohibits any carbon excess on the SiC surface, and then it requires an external carbon source (propane in our case) to grow graphene. Another interesting point is that depending on the growth conditions, the SiC surface can be more or less hydrogenated during graphene growth, allowing it to grow either a graphene monolayer on a buffer layer or a graphene monolayer on a hydrogenated interface. Also, no specific cleaning is required before graphene growth, as the ramp-up under hydrogen constitutes sufficient surface cleaning. The samples grown by CVD present full graphene coverage, with typical monolayer

cover in the 90 % to 99 % range v.s. 9 % to 1 % bilayer. All steps are 0.75 nm high, except around bilayer patches.

4.1.2 Device fabrication

Several samples have been processed by KRISS and CNRS using e-beam lithography. The process uses only PMMA as a resist to avoid any unwanted doping of the graphene. Care is also taken to cover the sample with a PMMA layer between each step to protect against air pollution. After the final deposition step of the gold pads for the bonding, a last lithography is performed in order to uncover the bonding pads leaving the graphene covered by PMMA.

As an alternative to the e-beam process, PTB has developed a UV lithography-based process which has the advantage of being much faster. The process initially proposed by the NIST has been further improved with respect to different wet- and dry-etching processes, metal compositions, and photoresists.

The Hall bar geometry has eight contacts of which six are Hall contacts, and two are the source and drain contacts. For the purpose of ac operation, the number of Hall contacts was reduced to the minimum number of six contacts that are required for the triple-series connection. Both the distance between two neighbouring contacts and the width of the graphene channel are 400 µm. Electrical contacting is realised by split-contacts (Figure 4.1.2) with eleven individual fingers in the case of the source/drain contacts and two fingers in the Hall contacts. The split contact helps to minimise the contact resistance of the device, and typical values, of the order of a few mΩ or even on the µΩ level, can be realised.

Since epitaxial graphene grown on SiC typically shows electron density in the 10^{12} to 10^{13} cm^{-2} range due to the doping from the buffer layer, a doping process is required to reduce the carrier density such that the quantum Hall effect can emerge at a lower magnetic field. The best results have been obtained by depositing multilayers of polymers including 2,3,5,6-tetrafluoro-tetracyano-quino-dimethane (F4-TCNQ). After spin-coating on SiC graphene, soft annealing processes were applied for diffusion of the hole dopants towards graphene. PTB has determined the electron density range where a quantised regime can be observed. The study shows particularly that electron density has to be reduced, but not below minimal values in the 5 to 10 × 10^{10} cm^{-2} range. The ideal carrier density to observe quantisation at the lower magnetic field (4 T) is also near this minimal electron density value (Figure 4.1.3).

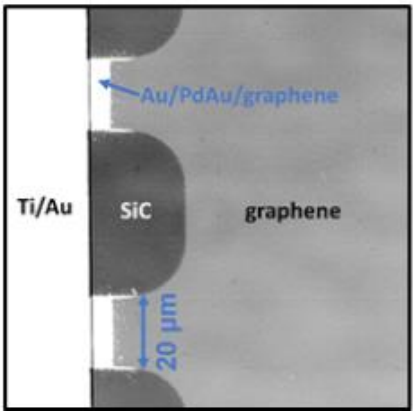

Figure 4.1.2: *SEM view of the split-contacts developed at PTB to minimise the contact resistance*

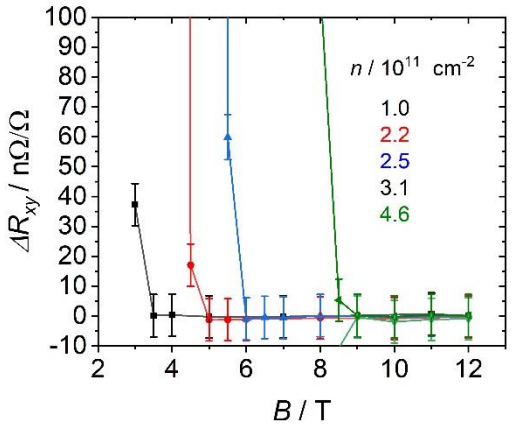

Figure 4.1.3: *Precision QH resistance at 4.2 K for devices with different carrier densities n. The ideal carrier density to observe quantisation at B<6T is between 1-2×10^{11} cm^{-2}*

4.1.3 DC characterisations

PTB and KRISS have produced many devices with low carrier density allowing us to obtain a relative accuracy of up to 10^{-9} at the required temperature and magnetic fields. Figure 4.1.4 shows, as an example, magnetotransport and precision measurements over time on a device from KRISS (stored in a glove box between measurements). The quantisation has been maintained over time above a magnetic field of 5 T at the liquid helium temperature of 4.2 K within the measurement uncertainty of a few nΩ/Ω.

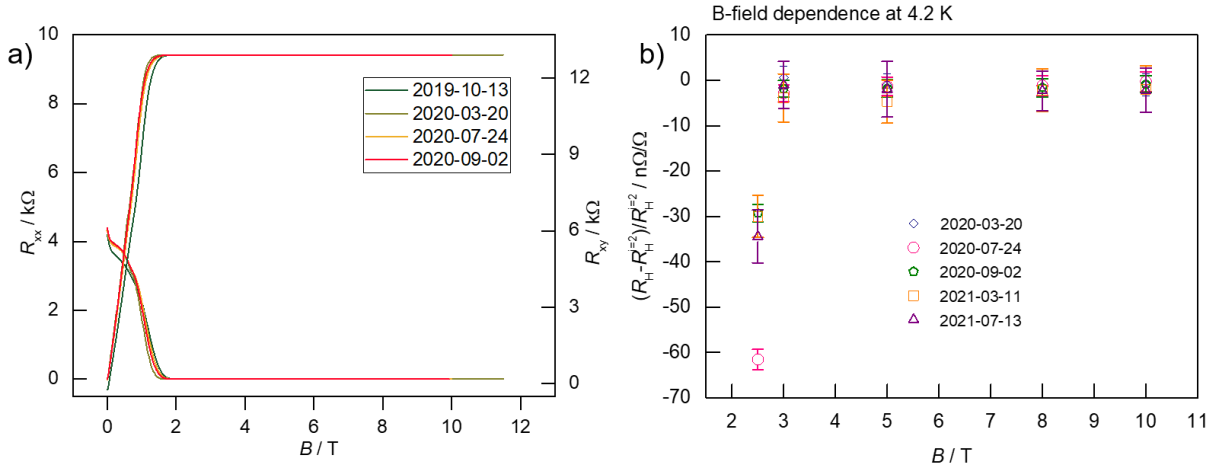

***Figure 4.1.4(a)**: Magnetoresistance measured at 2 K. **(b):** relative deviation of quantum Hall resistance at filling factor 2 from the nominal valve of $R_K/2$ at a temperature of 4.2 K. The error bar indicates the expanded measurement uncertainty (k=2)*

KRISS investigated the stability of a graphene device with an initial carrier density of 6 ×10^{10} /cm^2, stored under argon in a glove box for two years. The change rate of carrier density is approximately 0.04 %/d. The metrological quantisation was achieved at a magnetic field of 3 T and at a temperature of 4 K. The agreement of the quantised resistance with $R_K/2$ at direct current was smaller than the measurement uncertainty of 2 nΩ/Ω. The stability of the quantisation has been confirmed through multiple thermal cycles for two years. The degree of equivalence for the quantised resistance at $R_K/2$ above a threshold magnetic field was in the order of 1 nΩ/Ω at direct current even though the carrier density change rate was as large as 0.5%/d. The stability of the quantisation has also been observed in other devices after long range transportation through interlaboratory comparisons (KRISS, PTB, and back to KRISS; PTB, CMI, KRISS, and back to PTB…).

(ii) Temperature dependence and critical current

LNE tested the accuracy of the Hall resistance quantisation resistance in a device from PTB as a function of temperature, at a constant measurement current of 50 µA and at the magnetic flux density of 5 T, which corresponds to the minimum dissipation for this device. **Figure 4.1.5** shows the relative deviation of the Hall resistance at filling factor 2 from its nominal value $R_K = h / 2 e^2$, plotted as a function of temperature. No deviation to the quantised value are observed up to T = 6 K within a 2-σ uncertainty (k = 2).

LNE also tested the robustness of the Hall quantisation as a function of the measurement current in the same PTB device. Operation of QHR devices at the highest possible measurement current is essential to maximise the signal-to-noise ratio. **Figure 4.1.6** shows the evolution of the measured longitudinal resistance per square (left axis) with dc current at different temperatures, while the right axis represents the calculated values of the corresponding relative deviation of R_{XY} from $R_K/2$. The horizontal dashed line marks the threshold level of dissipation ($R_{XX} \leq$ 337 µΩ) above which the relative deviations of R_{XY} are expected to exceed 1 × 10^{-9}. At low temperature (T = 1.5 K), accurate quantisation of the Hall resistance is therefore expected for a measurement current below the value I_{max} of about 350 µA, while at moderate temperature (T = 4.2 K), $I_{max} \simeq$ 200 µA. At higher temperature (T > 6 K), a significant longitudinal resistance is measured even in the limit of a small measurement current, which therefore prevents accurate quantisation of the Hall resistance.

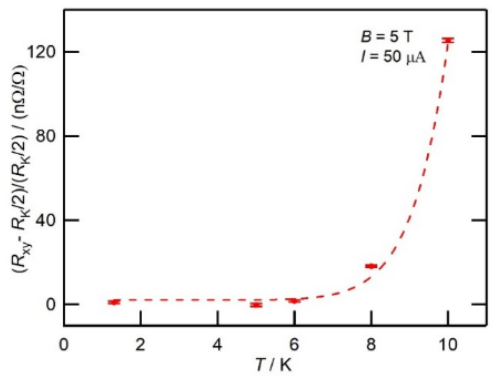

Figure 4.1.5: *Relative deviation of the quantum Hall resistance at filling factor 2 from the nominal value of $R_K/2 = h/(2e^2)$, as a function of temperature. The dashed line is a guide for the eyes [7]*

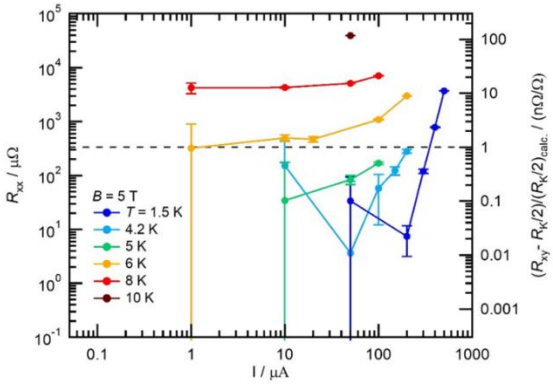

Figure 4.1.6: *Longitudinal resistance per square R_{xx} as a function of the measurement current at different temperatures (left axis) and corresponding relative deviation from its nominal value $R_K/2$ (right axis) [7]*

4.1.4 AC characterisations

The graphene devices to be investigated in AC were selected on the basis of DC measurements to check whether they fulfil the technical guidelines for DC. This is necessary, but not sufficient to reach the targeted uncertainty in the AC regime. Three out of the eleven most promising QHE devices were measured each at two institutes in AC. The first one was measured at METAS and afterwards at PTB, the second one at CMI and PTB, and the third one at CMI and KRISS. The remaining ones were measured in AC each in the lab of one of the partners (METAS, CMI, KRISS, INRIM, PTB) only.

(i) Longitudinal resistance

The CCEM technical guidelines on the reliable DC measurements of the quantised Hall resistance specify that the quantum Hall resistance must be measured on a two-dimensional electron gas (2DEG) in a dissipationless state, *i.e.* in a state of vanishing longitudinal resistance. Therefore, the longitudinal impedance measured on the QHE device is a key parameter for the determination of the quantisation state of the 2DEG. Figure 4.1.7(a) presents longitudinal resistance measurements at CMI at different temperatures (4.2 K and 2.5 K). As expected, the plateau width increases by lowering the device temperature. Figure 4.1.7(b) presents longitudinal resistance measurements at PTB at different frequencies when varying the

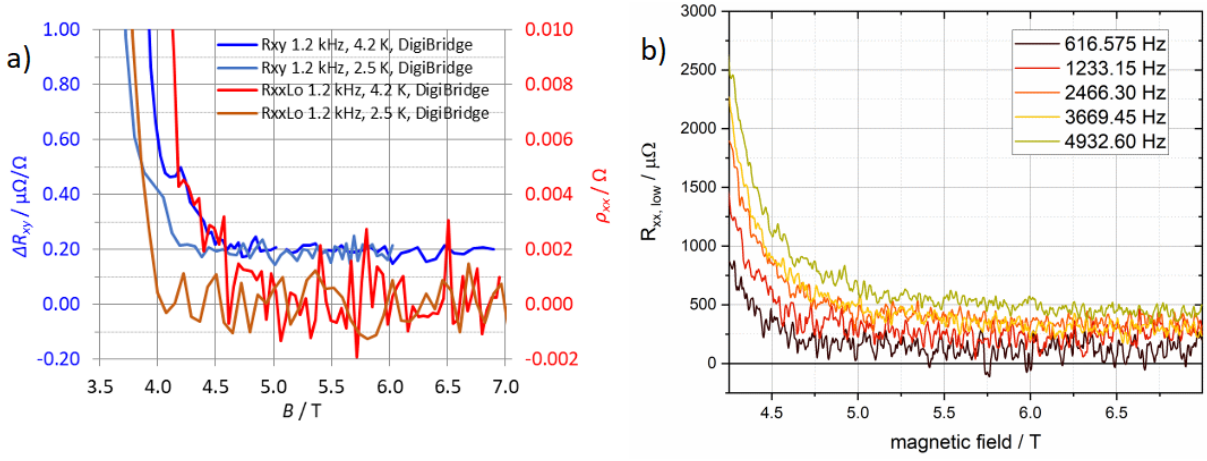

Figure 4.1.7(a)*: Measurement of plateau shape (R_{XY}) and longitudinal resistance (R_{XX}) at two different temperatures on a PTB device.* ***(b)****: longitudinal resistance at the low potential side of the same device at different frequencies, with 100 mV varying the magnetic field*

magnetic field. Similarly, the flat part of the longitudinal resistance with respect to the magnetic field gets smaller with increasing frequency. For a frequency of 616.575 Hz the longitudinal resistance remains constant between approximately 4.75 T and the maximum field of the system used of 7 T. For the highest measured frequency, the flat part starts around 6 T. Comparing these results from PTB to that first obtained at CMI agrees within the uncertainties of the two different measurement systems.

(ii) Measurements at kHz frequencies

At CMI, graphene QHR devices were measured mainly at 1.2 kHz using the bridge in both fully digital configuration and digitally assisted with an added reference inductive voltage divider for characterisation of graphene devices. This was done mostly against resistors with a calculable frequency dependence of 1 kHz. An example of plateau shape measurement at two temperatures is given in **Figure 4.1.8**(a). The observed deviation of about 0.2 µΩ/Ω is a range which is typical (up to few parts in 10^{-7}) for an unscreened device. The obtained plateau is flat within measurement uncertainties for magnetic fields above 4.75 T at 4.2 K and slightly before 4.5 T at 2.5 K. Another sample has been measured at a higher frequency of about 5 kHz and this showed a frequency dependent deviation between the measured resistance from the DC value (**Figure 4.1.8**(a)). In this measurement also the curvature of the plateau shape increases with frequency as known from GaAs devices.

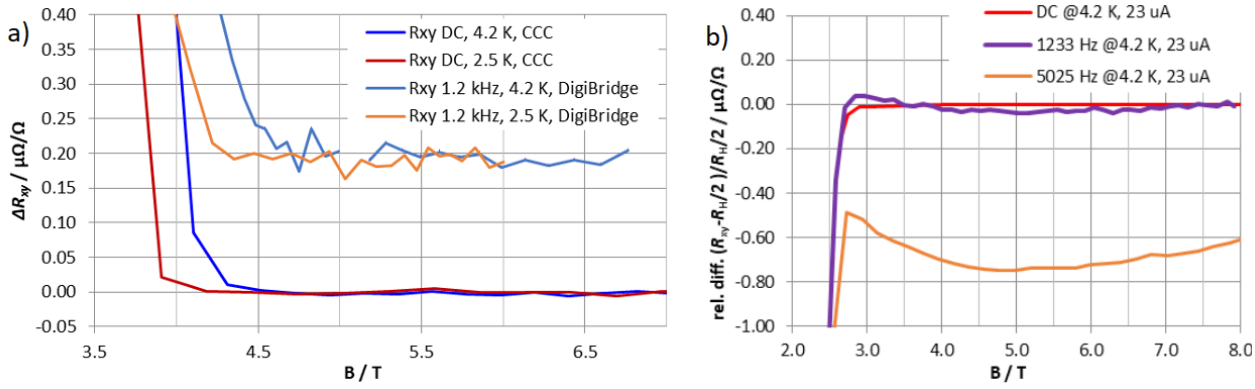

Figure 4.1.8: *Measurement of plateau shape at DC and AC at two different temperatures* ***(a)*** *and at two different frequencies* ***(b)*** *at CMI*

In total more than ten devices fabricated at PTB and KRISS were successfully measured at five project partners (METAS, CMI, KRISS, INRIM, PTB). Three of the most promising QHE devices were measured each at two institutes (METAS, CMI, KRISS, PTB). in AC. Even after long transportation, the obtained results showed no significant differences. Even though quite different setups (cryo-magnet systems, cryoprobes and impedance bridges) were used, the results obtained are in good agreement. Due to high interest of all partners, further device exchange between the institutes is planned and more details will be obtained.

Conclusion

The QHR is an important and reliable standard in DC metrology. The expected reliability of graphene-based devices combined with lower requirements for magnetic field and temperature may encourage more NMI's to use them as a resistance standard. Besides all these advantages, AC losses still need to be investigated and controlled. The applied different measurement methods and the results obtained convincingly show that resistance measurements with a relative accuracy of up to 10^{-8} are possible even for magnetic fields lower than 6 T and temperatures as high as 4.2 K in the low kHz range, which are the needed pre-conditions for traceability of impedance units to the QHE, and that the objective was achieved.

Even though the measurement setups and methods are different and long transportation was necessary, the results obtained showed no significant differences. The samples measured at a single institute also show very good results and they seem suitable for the traceability of impedance units to the QHE. All efforts of this project lead to the fact that the traceability of the impedance units from graphene-based AC-QHE is possible and that this capability can be transferred to other institutes.

4.2 Advanced digital bridges for the frequency range up to 100 kHz (Objective 2)

Introduction

With the 2019 redefinition of the SI, the QHE became the realisation of the resistance unit. To fully take advantage of this redefinition, the various impedance scales have to be realised directly from the QHR using fully automated bridges that are able to cover the entire complex plan up to frequencies of at least 50 kHz. Traditional transformer-based bridges are not suitable to be automated and are limited in frequency. Therefore, digital bridges, based on state-of-the-art ADC and DAC, and Dual Josephson Impedance Bridge (DJIB) have been developed and improved in this project. At the end of this project, this new class of bridges are fully automated, their accuracy is getting close to traditional bridges and their working frequency range has been expanded up to 100 kHz for digital bridges and to 50 kHz for DJIB.

4.2.1 Capacitance range from 10 pF to 10 nF

(i) CMI digital bridge

CMI has worked on improvements to the new capacitance traceability chain, consisting of the kHz frequency range and the 100 kHz range (Figure 4.2.1). The capacitance unit is realised from direct comparison of capacitance of a nominal value 10 nF to the known resistance standards of 12.9 kΩ or 10 kΩ at a frequency of 1.592 kHz, and respectively at a frequency of 1.23 kHz. A resistor with calculable frequency dependence is usually involved and its DC value is corrected for AC/DC difference.

An improved fully digital bridge (Figure *4.2.2*), developed at CMI, is used for R-C comparison. The bridge works on the principle of 1:1 impedance ratio comparison against ultra-stable digital synthesizers SWG. CMI improved automated evaluation of the bridge settings to achieve equilibrium state of 4-TP defined standards. It led to faster bridge balancing during R-C calibration and easier operation. Uncertainty of capacitance linkage of 0.07×10^{-6} F/F was achieved, where the uncertainty of the reference resistance standard is included. The main uncertainty source is related to phase matching due to the nonzero time constant of the reference standard. Such a bridge was later modified for operation with graphene-based AC QHR too, to remove resistance artefacts from the calibration chain.

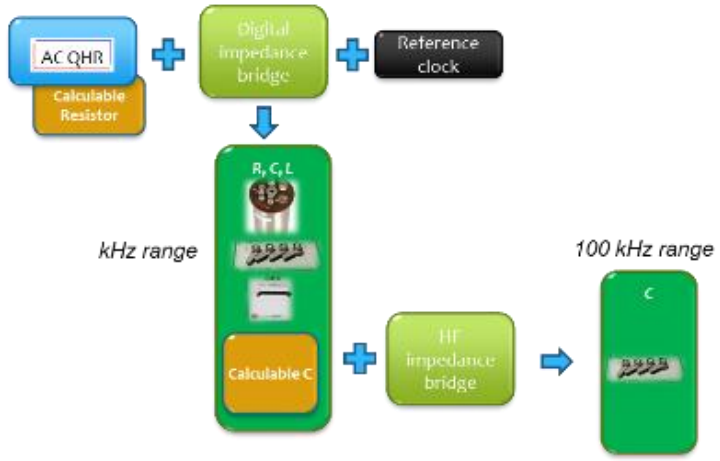

***Figure 4.2.1**. Proposed traceability of the capacitance unit for the kHz and 100 kHz frequency range*

For scaling of capacitance up to 100 kHz, a reference capacitance standard 10 nF calibrated in the previous step from R is used for sequential calibration of 1 nF and 100 pF capacitors using a digitally assisted bridge. The 100 pF capacitor is a calculable coaxial capacitor CXC100 developed prior the project at CTU in Prague and it serves for extension of the frequency range - its low-frequency value is correctable for its HF/LF difference. Then, the capacitance scale at 100 kHz is covered by means of 10:1 impedance ratio measurements performed with a high frequency digitally assisted bridge. The high-frequency bridge within the project was equipped with a new high-frequency generator and miniature auxiliary impedance decades. Therefore, better stability and faster balancing of the bridge was achieved, leading to easier operation of the bridge. The uncertainty of the capacitance scaling at 100 kHz is about 7×10^{-6} F/F and it fulfils the project's target for this type of bridge and frequency.

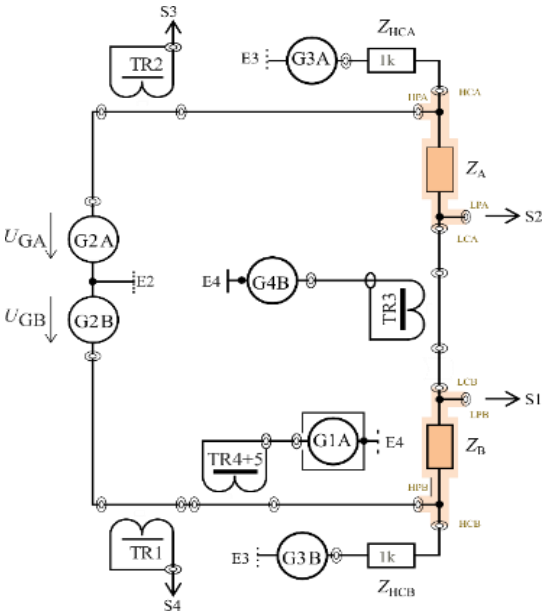

***Figure 4.2.2**. Simplified schematic of the R-C bridge. Ei denotes shared ground points; Si denotes detection points for a null detector*

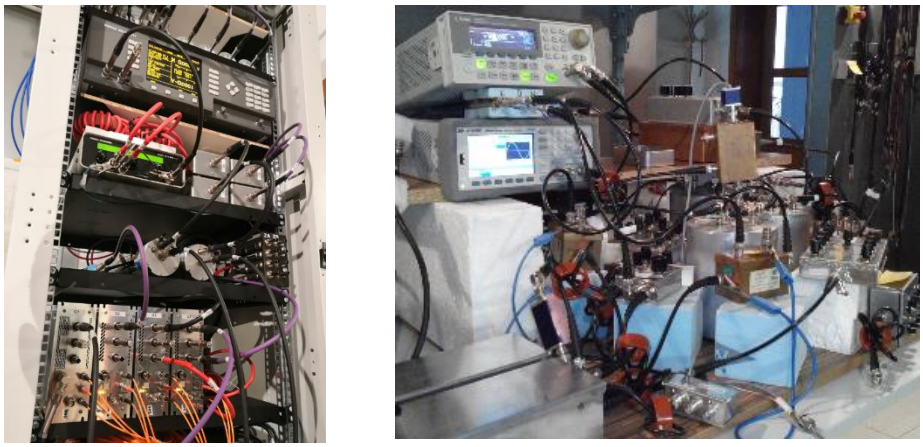

***Figure 4.2.3**. Left: Digi-Bridge for linking capacitance to the resistance unit. Right: High-frequency bridge with implemented new auxiliary decades and a DDS generator*

(ii) INRIM-POLITO fully-digital bridge

The 4-TP fully-digital bridge developed by INRIM and POLITO works according to the principle described in [3], which also provides a detailed description of the implementation and a preliminary evaluation of the uncertainty.

The principle schematic of the bridge is represented in Figure 4.2.4 and a picture of the implementation is shown in Figure 4.2.5. The bridge is balanced when the voltages at the ports LP1, LP2, DHP1 and DHP2 are zero. When the bridge is balanced, the ratio Z_1/Z_2 can be determined from the voltages E_1, E_2, E_0 and the impedance Z_0, according to the measurement model reported in [4].

The two impedances under comparison, Z_1 and Z_2, can be of different type and magnitude but the bridge is optimised to yield the best uncertainty when the ratio magnitude is approximately one, that is, $|Z_1/Z_2|\approx 1$.

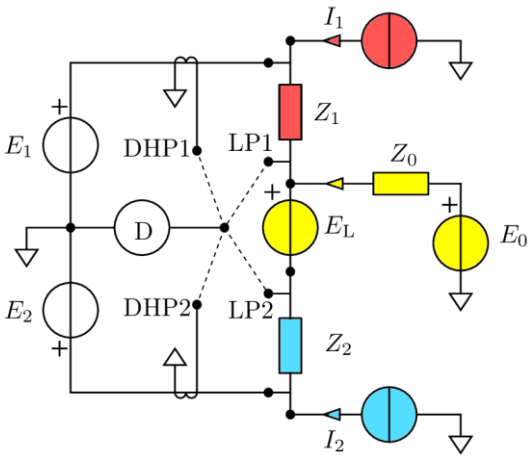

***Figure 4.2.4**.*

INRIM-POLITO bridge principle schematic

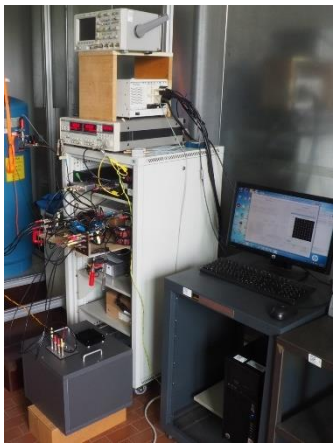

***Figure 4.2.5**.*

Picture of the INRIM-POLITO bridge

- **Traceability chain for the farad**

The traceability chain that is being developed at INRIM starts, as shown in Figure 4.2.6, with the calibration of an 8 nF standard capacitor from an AC quantised Hall resistance standard by means of the fully-digital bridge described in section 3.1, operating at about a 1541 Hz frequency, at which the impedance ratio magnitude is about 1.

The 8 nF capacitance is then scaled to 1 nF by means of a transformer ratio bridge and then to 100 pF and 10 pF by means of a capacitance build-up method.

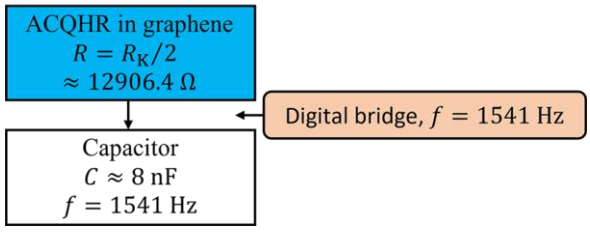

***Figure 4.2.6**. INRIM traceability chain to calibrate an 8 nF standard capacitor from an AC quantised Hall resistance standard*

- **Bridge uncertainty**

Table 4.2.1 below reports an uncertainty budget for the INRIM fully-digital bridge for a comparison between a standard resistor R≈12.9 kΩ and a standard capacitor C≈8 nF at the frequency f≈1541 Hz. At this frequency, $|Z_1/Z_2|=2\pi fRC\approx 1$. Table 4.2.1 reports the standard uncertainty (k=1) for the quantity $\Delta=\mathrm{Im}(Z_1/Z_2)-1=2\pi fRC-1$. The total standard uncertainty is therefore at the level of 10^{-7}, within the target of the project for this type of bridge.

Table 4.2.1 Uncertainty budget of the INRIM fully-digital bridge for a comparison between a 12.9 kΩ standard resistor and an 8 nF standard capacitor at 1541 Hz

Quantity i	$u_i(\Delta)\times 10^6$
Bridge reading	0.022
Crosstalk	0.089
Injection	0.01
Total RSS	0.092

(iii) KRISS digital bridge

KRISS has extended the frequency of the 4-TP digital bridge from CMI up to 100 kHz, and the bridge measurement uncertainty has been evaluated mainly at 1 kHz for the capacitance measurements. The bridge can be configured in a digitally assisted mode with a ratio transformer as shown in Figure 4.2.7 to compare standard capacitors in 10:1 ratio. The measurement uncertainty was evaluated for the 100 pF:10 pF case as shown in Table 4.2.2 at 1 kHz. The uncertainties from the imperfect coaxiality and lead wire corrections were estimated to be at the level of 10^{-9}. On the other hand, the uncertainties for the bridge resolution and sensitivity, the measurement repeatability, and the transformer voltage ratio were at the level of 10^{-8}. When all combined, the bridge measurement uncertainty was about $5.4 \cdot 10^{-8}$. For the calibration uncertainty of 10 pF, the uncertainty for the 100 pF reference value will be added together with its short-term stability from the temperature stability, for instance.

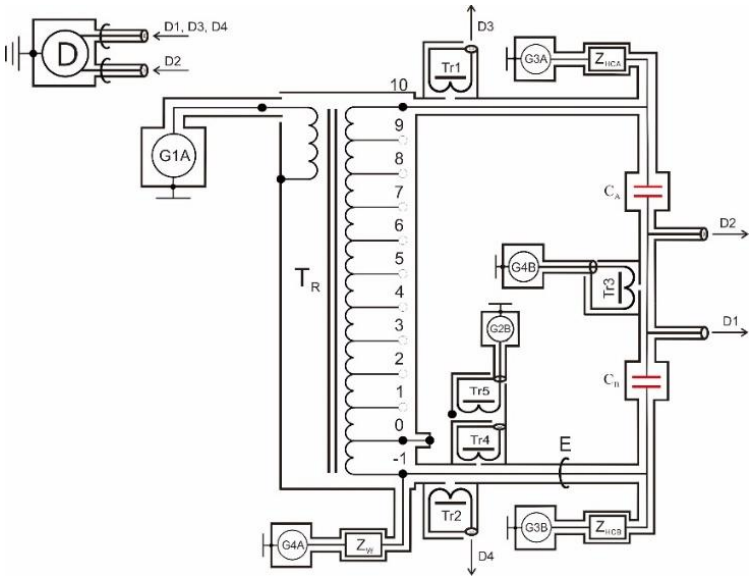

Figure 4.2.7. *Simplified schematic of the digitally assisted 4-TP bridge for C-C comparison*

Table 4.2.2 *Contribution of the sources of uncertainties for 100 pF: 10 pF capacitance ratio measurement with the digitally assisted 4-TP bridge at a 1 kHz frequency*

Quantity *i*	$u_i(C_A/C_B)$ $\times 10^6$
Transformer ratio	0.040
Bridge resolution/sensitivity	0.025
Bridge coaxiality	0.008
Lead corrections	0.003
Repeatability	0.025
Combined u	0.054
Expanded U	0.108

The capacitance unit can be traced from the DC QHE via a calculable resistor and digital bridges. For instance, 10 kΩ AC resistance traced to the DC QHE can be compared with the 10 nF capacitance using the fully digital quadrature bridge. Thus calibrated 10 nF can be scaled down to 10 pF using the 10:1 ratio digital bridge.

4.2.2 Dual Josephson Impedance bridge for the range up to 100 kHz

(i) The METAS Josephson Impedance bridge (DJIB)

Recently, a new generation of fully digital bridges have been developed that use two independent Josephson Arbitrary Waveform Synthesizer (JAWS) voltage sources to generate accurate arbitrary voltage ratios. A JAWS is a perfect digital-to-analogue converter that produces a calculable, distortion free voltage waveform with quantum-based accuracy over frequencies between a few hertz and 1 MHz or at DC. The DJIB was designed to accurately determine the ratio of any two impedance standards defined as four-terminal-pair standards. The frequency ranges from less than 1 kHz up to 80 kHz and the maximum rms amplitude used in this work is 0.3 V. The bridge is fully computer controlled, though the operator must still manually change the connections between the impedances and the bridge. The DJIB can be divided into two distinct parts:

- The dual JAWS system, which generates two independent sine waves at the required frequency, amplitudes, and phases. The JAWS system is controlled by its own computer.
- The bridge, which is composed of detection and injection transformers as well as the different analogue-to-digital convertors (ADCs) and DACs needed to measure the state of the bridge and trim the bridge balance, respectively. A second computer controls the bridge measurement sequence and iteratively tunes the JAWS output voltages and DACs to balance the bridge.

Figure 4.2.8 shows a detailed schematic of the DJIB. A full description can be found in [Overney, F. et al., Metrologia, 57/6, 065014 , 2020].

When the bridge is balanced, the impedance ratio is directly given by: $$\frac{Z_{\mathrm{bot}}}{Z_{\mathrm{top}}} = -\frac{V_{\mathrm{bot}}}{V_{\mathrm{top}}} = -V_{\mathrm{ratio}},$$

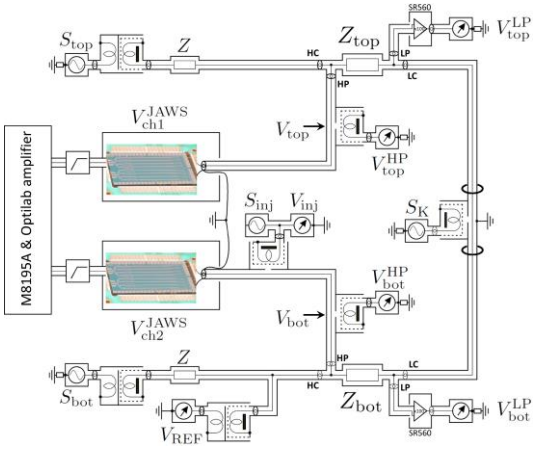

Figure 4.2.8. *Schematic of the Dual Josephson Impedance Bridge (DJIB). The two four terminal-pair impedance standards to be compared (Z_{top} and Z_{bot}) are connected in series. Once the bridge is balanced, the impedance ratio is equal to the voltage ratio*

Table 4.2.3: *Uncertainty budget of the DJIB for different frequencies. The uncertainties are given as a relative uncertainty in $\mu\Omega/\Omega$ with a coverage factor of k=1. A detailed explanation of the various sources of uncertainty is presented in [Overney, F. et al., Metrologia, 57/6, 065014 , 2020]*

Ratio 1:1

Uncertainty component ($\mu\Omega/\Omega$)	1 kHz	20 kHz	60 kHz
(a) Bridge resolution	0.009	0.013	0.032
(b) Cable correction	0.004	0.015	0.125
(c) Voltage injection chain	<0.001	<0.001	0.006
(d) Quantum locking range	<0.001	<0.001	<0.001
Combined (k=1)	**0.010**	**0.020**	**0.129**

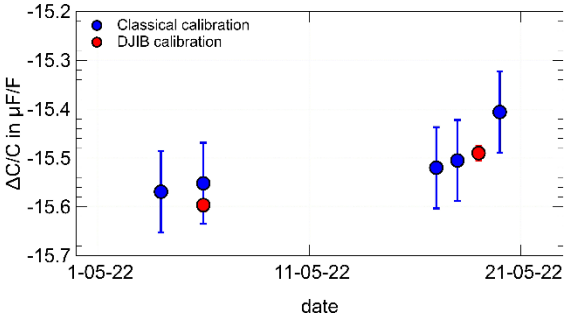

Figure. 4.2.9. *Calibration of a 10 nF capacitor performed at 1233.147 Hz using either the classical calibration chain or by direct comparison to calibrated resistance standards using the DJIB*

As a validation test, the calibration of a 10 nF capacitance standard has been performed at 1233.147 Hz by direct comparison to a calibrated resistance standard using the DJIB. The same capacitance standard has also been calibrated using the classical calibration chain in operation at METAS. Figure 4.2.9 shows the good agreement between the two sets of calibration results. The uncertainty bars represent the k = 1 uncertainty. The uncertainty is about 0.08 μF/F for the classical calibration and less than 0.02 μF/F the DJIB calibration.

(ii) The PTB Josephson Impedance bridge

The four terminal-pair (4TP) Josephson impedance bridge of PTB was developed over the last years starting as a two-terminal pair impedance bridge for ratio and quadrature measurements with rms amplitudes of up to 20 mV. Also, in this first stage it was used in combination with QHR devices, this time in GaAs [S. Bauer et al., Metrologia 54, 2017]. Within the project this system was extended to a four-terminal pair definition as shown in Figure 4.2.10. The maximum amplitude is now 100 mV in a frequency range between 50 Hz and 50 kHz.

(a)

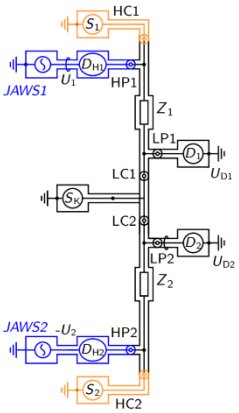

(b)

Figure 4.2.10. *(a) Picture of PTB's 4TP Josephson impedance bridge. (b) Simplified schematic of 4TP Josephson impedance bridge setup comparing two impedance standards*

When the bridge is perfectly balanced, U_{D1} and U_{D2} are zero and the impedance ratio is given by

$$\frac{Z_2}{Z_1} = \frac{U_2}{U_1}. \quad (1)$$

Like the METAS DJIB, PTBs bridge can be divided into two distinct parts:

- The dual JAWS system, which generates two independent sine waves at the required frequency, amplitudes, and phases.
- The bridge setup consists of injection and detection transformers, automatic switches to reverse the applied Josephson voltages. In contrast to the METAS system this system uses a lock-in amplifier instead of ADCs and both parts are controlled by the same computer.

To evaluate the performance of the Josephson impedance bridge, ratio measurements using two 10 nF capacitance standards and 10 kΩ and 12.9 kΩ resistance standards were carried out. The results were

compared to one of the most accurate impedance bridges based on inductive voltage dividers at a frequency range from 53 Hz to 50 kHz. The ratio of two 10 nF capacitance standards and the ratio of 12.9 kΩ and 10 kΩ resistance standards were measured as shown in Figures 4.2.11 and 4.2.12 respectively. The estimated uncertainties for these ratio measurements at 1233.15 Hz are listed in Tables *4.2.4* and *4.2.5.*

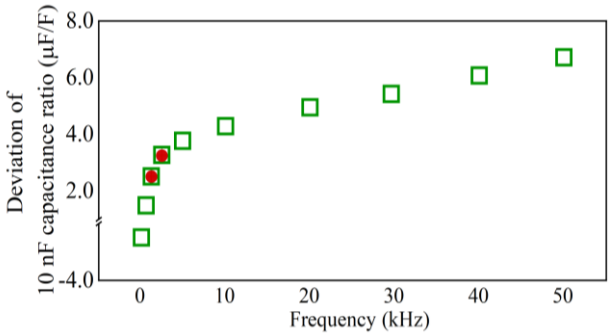

Figure 4.2.11. *Deviation from the 1:1 ratio of two 10 nF capacitance standards measured by the 4TP Josephson impedance bridge with 100 mV (☐) and by PTB's IVD bridge (●)*

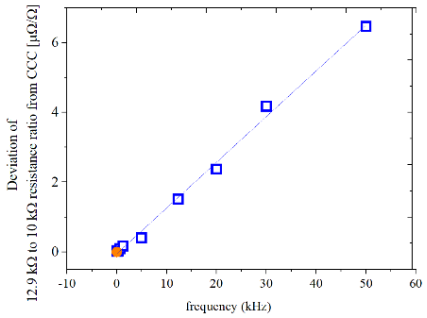

Figure 4.2.12. *Deviation of ratio of 12.9 kΩ and 10 kΩ resistance standards measured by the 4TP Josephson impedance bridge (☐) from Cryogenic Current Comparator (CCC) (●). The linear fit of 4TP bridge values at DC measurement shows good agreement with CCC*

Table 4.2.4. *Uncertainty budget of PTB's Josephson impedance bridge for a 1:1 ratio of two 10 nF capacitance standards with measurement at 1233.15 Hz (k = 1)*

Quantity (x_i)	**Uncertainty Contribution** $u(y_i) = \lvert c(x_i) \rvert \times u(x_i)$ **Relative**
Bridge resolution	3.0 nF/F
JAWS voltage	2.9 nF/F
Cable corrections	4.6 nF/F
Bridge deviation	2.9 nF/F
Kelvin network	1.2 nF/F
Combined uncertainty	u_c = 7 nF/F

Table 4.2.5. *Uncertainty budget of PTB's Josephson impedance bridge for a ratio of 12.9 kΩ and 10 kΩ resistance standards with measurement at 1233.15 Hz (k = 1)*

Quantity (x_i)	**Uncertainty Contribution** $u(y_i) = \lvert c(x_i) \rvert \times u(x_i)$ **Relative**
Bridge resolution	4.0 nΩ/Ω
JAWS voltage	2.9 nΩ/Ω
Cable corrections	5.8 nΩ/Ω
Bridge deviation	3.5 nΩ/Ω
Kelvin network	1.2 nΩ/Ω
Combined uncertainty	u_c = 9 nΩ/Ω

Conclusion

Different types of digital impedance bridges were upgraded and evaluated in detail in the labs of the partners: INRIM's fully digital bridge with support from POLITO, CMI's digitally-assisted and fully-digital bridge, KRISS' digitally-assisted bridge. The evaluation and optimisation of the bridges has led to lower uncertainties, higher stability and faster balancing of the bridges. The obtained accuracy for capacitance calibration of 10 nF and 10 pF capacitors, respectively, was better than the originally expected targets. A relative uncertainty of 7×10^{-8} was achieved at 1.2 kHz and even at 100 kHz the uncertainty reached 7.3×10^{-6}. Also the two dual Josephson impedance bridges in the project were upgraded and evaluated: at METAS and at PTB with support from NIMT. These very versatile instruments are spanning a frequency range from 50 Hz to 60 kHz. The comparison to the conventional impedance bridges showed a very small deviation of $(2\pm7)\times10^{-9}$ at the highest frequency for the link of a 10 nF capacitance standard to the quantum Hall resistor and indicated that the objective was met.

4.3 Combination of graphene devices with impedance bridges and traceability of capacitance to the QHE (Objective 3)

The combination of graphene QHR devices with a Josephson impedance bridge or with a fully digital bridge will lead to a simplified traceability for capacitance and AC resistance standards to the QHE in the AC regime. The combinations of graphene quantum Hall devices with digital impedance bridges will give a broad field of application in NMIs all over the world. The combination with Josephson impedance bridges gives a realisation in which all references have a fully quantum nature.

In a first step appropriate cryo probes for AC measurements were developed by INRIM, CMI, KRISS, METAS, LNE and PTB. The cryo probes and the suitability of the shielded TO-8 sample holder were successfully tested at the corresponding institutes. With this, the principal requirements for the successful evaluation of the graphene-based impedance standards in combination with the developed impedance bridges were supplied.

4.3.1 Josephson impedance bridge

The main goal of this project is to improve the impedance scale by comparing a capacitance standard directly to a graphene sample using Josephson Impedance Bridges (DJIB). The experimental setup at METAS can be seen in Figure 4.3.1 and those of PTB's system is shown in section 4.2.2.

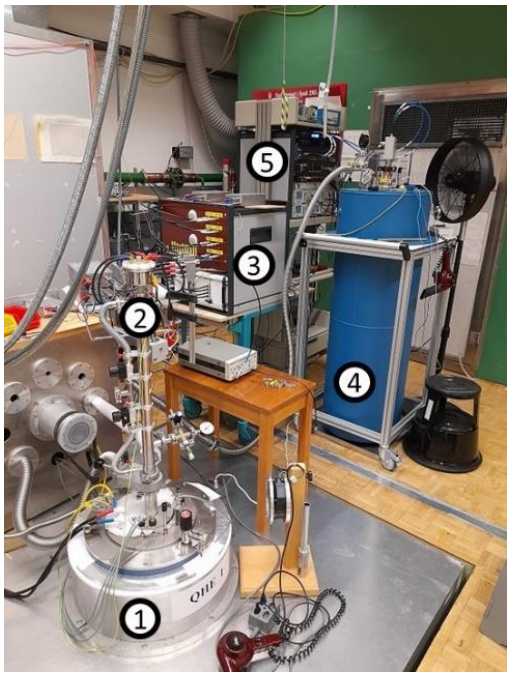

Figure 4.3.1: *Picture of the system showing its main components: (1) LHe cryostat hosting the graphene quantised Hall impedance at 4.2 K in high magnetic field (up to 12 T), (2) Coax cryoprobe connecting the device to the bridge, (3) Fully automated digital impedance bridge, (4) LHe cryostat with dual pulsed Josephson junction arrays, (5) Electronics of the Josephson arbitrary waveform synthesizer, (6) Capacitor (not visible)*

The major result of the project obtained at METAS is depicted in Figure 4.3.2, where the capacitance scale realisation is shown for three different comparison methods:

- The classical method is based on a traditional inductive voltage divider bridge and a high precision ratio transformer. A pair of well characterised Gibbings resistors is compared to a pair of 10 nF capacitors with the quadrature bridge at a frequency of 1233 Hz. Each point (blue) in Figure 4.3.2 represents a full day of manual measurements.
- The same Gibbings resistors are directly compared to a 10 nF capacitor using the DJIB. Each point (red) in Figure 4.3.2 represents less than 2 hours of fully automated measurements and fully agrees with the classical method. In addition, the measurement uncertainty obtained with the DJIB (0.03 ppm) is one order of magnitude smaller.
- The 10 nF capacitor is directly compared to a graphene quantum Hall device. This result is the first comparison of this type at METAS. Only PTB and METAS can perform this kind of measurement worldwide. As can be seen in Figure 4.3.2, there is a difference of 1.7 ppm between this data and the two previous methods. Of course, this discrepancy is presently under investigation. It is worth noting that the type A uncertainty of the graphene comparison is smaller than the Gibbings comparison due to a reduction of the Johnson noise in the graphene device that is cooled down to 4.2 K.

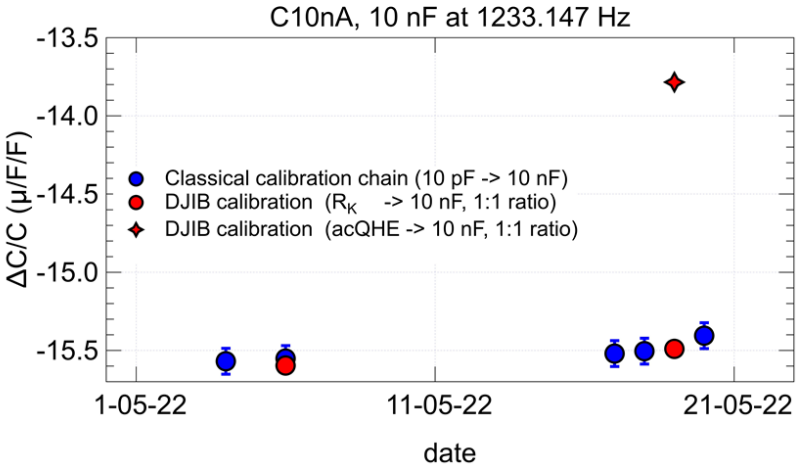

Figure 4.3.2: *Calibration of a 10 nF capacitor performed at 1233.147 Hz using either the classical calibration chain (blue dot), the direct comparison to a calibrated resistance standard using the DJIB (red dot) or a direct comparison to a graphene quantised Hall resistor using the DJIB (red star)*

The CCEM technical guidelines on the reliable DC measurements of the quantised Hall resistance specify, among other recommendations, that the quantum Hall resistance must be measured on a two-dimensional electron gas (2DEG) in a dissipationless state i.e., in a state of vanishing longitudinal resistance. Therefore, the longitudinal impedance measured on the QHE device is a key parameter for the determination of the quantisation state of the 2DEG. Although the measurement of the longitudinal resistance is relatively straightforward in DC, the situation is significantly more complicated in AC.

For this reason, a new bridge was developed at METAS, which allows the direct measurement of the in-phase and out-of-phase components of the longitudinal voltage drop on the low-potential side of the QHE device. The bridge gives access to the complex longitudinal impedance $Z_{xx} = R_{xx}+j\omega L_{xx}$ (where $j = \sqrt{(-1)}$ and ω is the angular frequency). The results obtained for R_{xx} with this new system show perfect quantisation (i.e. a dissipationless state) below 7 T. As soon as the frequency is increasing, the dissipation in the 2DEG is increasing as well. However, it is worth noting that this level of dissipation is fully compatible with uncertainties at the level of 0.01 μΩ/Ω on the Hall impedance. These data, and in particular the L_{xx} measurements, are still under evaluation.

The combination of PTB's 4-TP Josephson impedance with a quantum-Hall resistance (GaAs or graphene) is setup, tested and operated in close collaboration with NIMT. To fulfil the defining conditions of a 4-TP measurement, the current within the high potential lines is minimised by adjusting the associated currents in the current high lines. This is repeated after each change in the voltage ratio between the two JAWS systems. The so-called main balance is reached when the reading of the main detector is nulled. This is achieved by adjusting the voltage ratio and phase angle between both Josephson systems. As already mentioned above, the use of a Kelvin balance is not needed since the triple-series connections ensure that the current within the potential lines at the low side is almost zero.

To investigate the noise/statistical uncertainty of the combined system, Allan deviation measurements with a QHR and impedance standards were carried out. The results are in perfect agreement with the theoretical expectation. Which proves that no additional and unexpected noise is generated by the setup itself. This combination was used within the project mainly to investigate the properties of the produced graphene QHR samples. For this purpose, temperature-controlled resistance and capacitance standards were used. One example is the measurement of the plateau flatness for which the impedance bride is balanced with a QHR as one, and a sufficiently stable reference standard as a second impedance, while the QHR is operated at a certain magnetic field. The latter is typically 7 T for the three samples investigated at PTB. When the bridge is balanced the magnetic field is changed with a slew rate (typ. < 0.1 T/min) and the change at the main detector is recorded. From this change the resistance of the QHR can be calculated as presented in Figure 4.3.3.

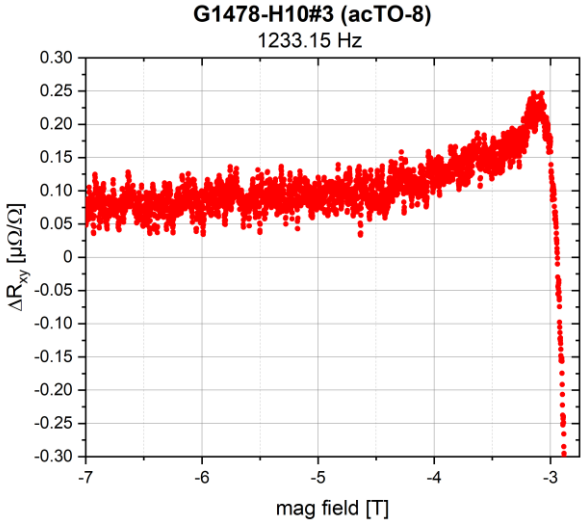

Figure 4.3.3: *Deviation of the measured resistance from the DC value over the magnetic field. The measurement was carried out at 1233.15 Hz against a 10 nF capacitance which was traced back to a GaAs quantum Hall resistance. The sample G1478-H10#3 was produced at PTB and installed into a double-shielded acTO-8 carrier (no applied shield potential during measurement)*

4.3.2 Full digital bridge

INRIM's travelling electronic impedance bridge was moved to PTB to be compared with the PTB's Josephson impedance bridge. This work was done in collaboration with POLITO in the frame and by support of EMPIR's Research Mobility Grant (RMG1). Figure 4.3.4 shows the implementation of INRIM's and PTB's bridges in the same laboratory at PTB. A 12.9 kΩ resistance standard and a 10 nF capacitance standard were employed as temperature controlled calibrated impedance standards in the technical assessment of the bridges. A graphene AC QHR device fabricated by PTB was characterised in both the DC and AC regimes and measured with both bridges against the temperature-controlled impedance standards. The technical assessment of the bridges was performed by means of the triangle measurements at 1233 Hz. The 10 nF capacitance standard was first calibrated directly against the graphene AC QHR and then against the 12.9 kΩ resistance standard in turn calibrated against the graphene AC QHR standard. This procedure was performed with both INRIM's and

PTB's bridges. For each bridge, the results of the two calibrations were compared to evaluate the self-consistency of the bridge measurements. A mutual validation of the bridges was then performed by evaluating the discrepancies between the calibrations of the standards obtained with the two bridges. The evaluation of the results was performed with support of POLITO which supplied numerical analysis models as well as circuit modelling and simulations of the impedance bridge. The successful comparison of the bridges resulted in an agreement within a few parts in 10^8 with a combined type A uncertainty of the same order.

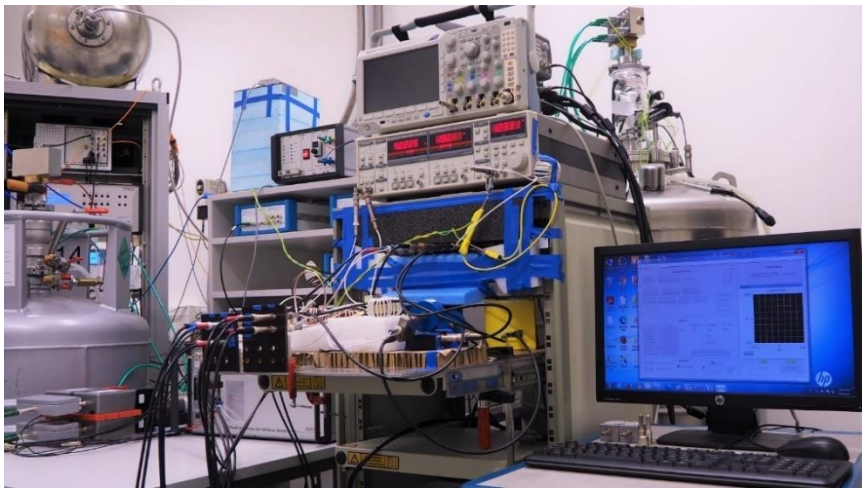

Figure 4.3.4: *Implementation of INRIM's (right) and PTB's (left) digital impedance bridges in the same laboratory at PTB. The Dewars on the right and on the left are the cryogenic systems hosting the graphene AC QHR and the JAWS device, respectively*

CMI has based the traceability chain of the capacitance unit on a fully digital bridge incorporating triple series connection of a graphene device as a reference standard and reference clock. The developed bridge achieved uncertainty below 0.07×10^{-6} for linking a 10 nF capacitor to 12.9 kΩ at 1233 Hz. Within two measurement steps, where forward and reversal impedance ratio measurement are performed at a frequency of 1233 Hz, data for the calculation of the capacitance value are obtained. In both forward and reversal measurements the same voltages of the main ratio arms are maintained, and the bridge is rebalanced by an additional synthesizer.

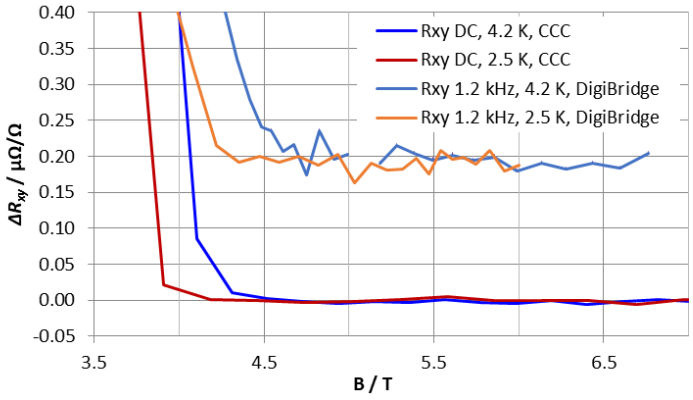

Figure 4.3.5: *Measurement of plateau shape of G1536-77-4 (PTB) at two different temperatures*

An automated balancing procedure was improved, so only the main bridge voltage needs to be set by the user prior to the measurement. To eliminate cable effects, the bridge is operated in a four-terminal-pair configuration. The achievable accuracy for a general 1:1 ratio was verified by means of capacitance measurements with agreement of 0.03×10^{-6}, while the Allan deviation of the ratio was below 0.01×10^{-6}.

The CMI bridge was used in both fully digital configuration and digitally assisted with an added reference inductive voltage divider for characterisation of graphene devices too, mainly against resistors with calculable frequency dependence, in a frequency range above 1 kHz. An example of plateau shape measurement at two temperatures is given in Figure 4.3.5.

KRISS's current traceability chain of the capacitance unit starts with a DC QHR. This is shown in the left chain of Figure 4.3.6. Within the GIQS project, the 12.9 kΩ AC-DC calculable standard resistor was compared with an AC QHR in 1:1 ratio using a digitally assisted (DA) coaxial bridge. The measurement value agreed in the level of 10^{-8} when compared with the reference value from DC QHR. Also, a fully digital (FD) quadrature bridge has been studied for the direct comparison of *R*-*C*. The FD quadrature bridge can directly calibrate 1 nF based on 103 kΩ. The measurement uncertainty for the 1 nF capacitance from the 103 kΩ resistance is evaluated to be about 5.0×10^{-7} ($k = 1$) when using the FD quadrature bridge. Furthermore, with the FD quadrature bridge, the right chain in Figure 4.3.6 is also possible, employing resistance standards of decimal nominal values.

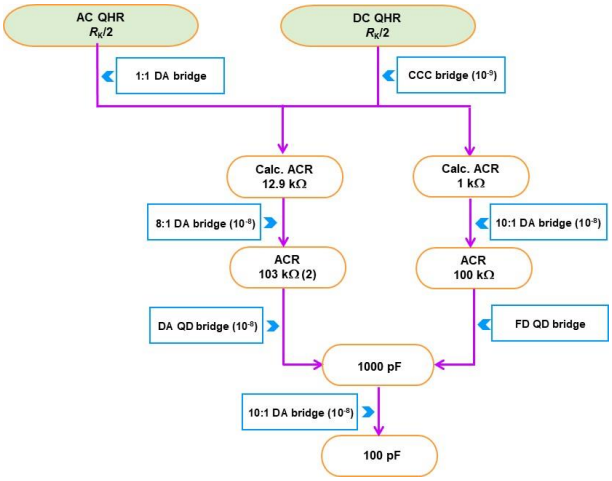

Figure 4.3.6: *KRISS Traceability chain for a 100 pF standard capacitor from DC and AC QHR standards*

4.3.3 Conclusion

The combination of a graphene QHR device with digital or Josephson impedance bridge was realised at five institutes (CMI, INRIM, KRISS, METAS and PTB) within the GIQS consortium. All these combinations worked successfully and the targeted uncertainties of about 0.1 μΩ/Ω for those combinations with digital impedance bridges and around 0.01 μΩ/Ω for those with Josephson impedance bridges were reached. The desired objectives were fully reached. Moreover, all these combinations were used to investigate the QHR devices from KRISS and PTB with respect to their operating parameters and metrological suitability.

4.4 Development and investigation of a cryo-cooler system hosting the superconducting Josephson device and the graphene device (Objective 4)

Recent progress in graphene-based quantum standards, Josephson Arbitrary Waveform Synthesizers (JAWS), Josephson impedance bridges, and cryogen-free refrigeration methods based on pulse tubes, have brought quantum standards much closer to applications outside NMIs. Even a universal quantum standard (UQS), a single setup to provide quantum traceability for all electrical units – voltage, current, resistance, impedance – at DC and audio frequencies, has become feasible.

A major challenge that must be solved before the UQS can be realised is to enable simultaneous operation of a QHR and a Josephson voltage standard (JVS) in the same cryostat. The difficulty arises because the QHR requires a high magnetic field that the JVS cannot tolerate. The problem has been fundamentally relieved by

the development of graphene-based quantum standards that operate at a much lower magnetic field than the presently used GaAs-based devices.

Two alternative solutions were developed. One of them – the VTT system – is a custom-made setup based on an existing pulse-tube refrigerator, and the other one – the RISE system – is based on a new commercial dry cryostat system which was modified to fit the needs to host both quantum systems simultaneously.

4.4.1 Cryo-cooler system

The original goal of VTT was to use an existing 0.7 W pulse tube (PT) cryocooler and an integrated helium liquefier as the cooling system. The unique advantage of this apparatus is its extremely low noise caused by mechanical vibration thanks to the non-solid connections of the PT to the cold stages of the cryostat. Unfortunately, the He gas mediated cooling of the 50 K stage proved to be too weak for cooling the magnet current wires. To solve this issue, VTT and *ICEoxford Inc*. (UK) started a collaboration with the aim to rebuild the cryostat making use of *ICEoxford*'s proprietary technologies related to low-vibration cryostats, liquefiers and superconducting magnets. A cryostat was designed to implement a dry 8 T magnet with an experimental chamber in the bore and up to three magnetically shielded experimental chambers in a compact space. Figure

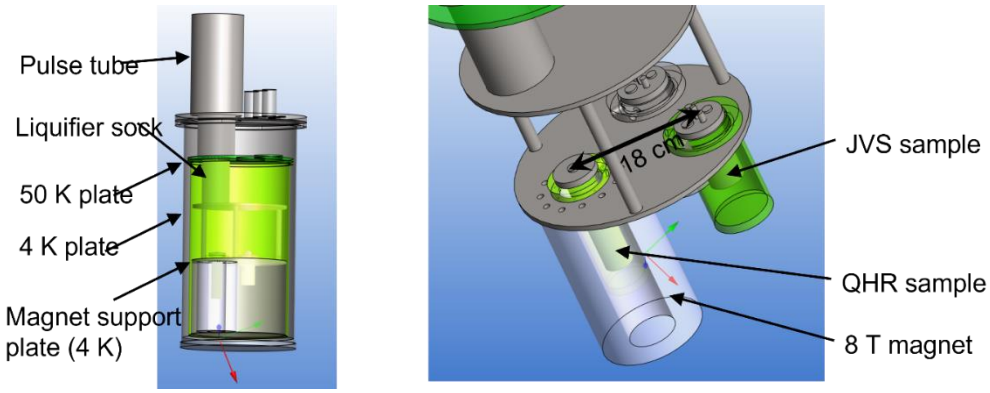

Figure 4.4.1: *Simplified diagram of the cryostat designed and under construction*

4.4.1 shows an illustration of the basic design. Two QHR chips can be mounted inside the magnets bore and the system can be extended by a 1.5 K pot.

For the JVS devices two alternative locations are planned: first, there are two magnetically shielded chambers next to the magnet (attached to the magnet support plate) and one attached to the 4.K plate. All these chambers can be filled with liquid helium. The cryostat has been designed to be compatible with a larger PT with 1 W cooling power (at 4.2 K) and a full vibration isolation system of *ICEoxford*. This modification would then also allow the building of a 1.5 K ^{4}He pot for the QHR operation at a lower magnetic field.

The distance between the axis of the magnet and the JVS chambers next to the magnet is only 180 mm which allows the use of short electrical connecting cables between the experiments, which significantly reduces cable corrections e.g. in impedance measurements. An obvious challenge of this design is that the JVS experiments are located in a region where the stray magnetic field is much higher (0.1 T to 0.4 T) than in usual JVS realisations. Typically, Josephson voltage standards are operated at some tens of nT residual field inside a Cryoperm cylinder. To realise this strong field reduction (of the order of 10^7), passive multilayer shielding

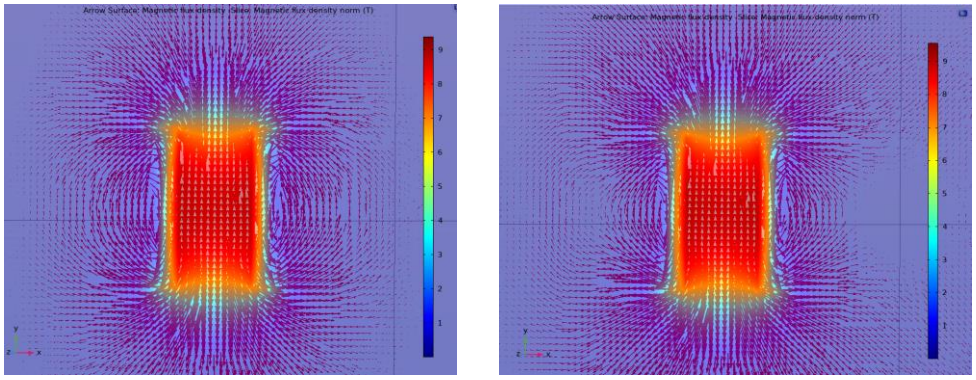

Figure 4.4.2. Left: *Full 8 T field of a simplified homogenous solenoid (not featuring the details of the superconducting magnet by ICE).* ***Right:*** *The same as before, but with a compensating field added by a copper coil surrounding the OVC to create a depleted field region seen right of the magnet*

designed as a two- or three-layer magnetic shielding structure is needed. The outermost layer will be made of a medium-permeability material ($\mu_r = 1000$) with high saturation (2.2 T) and inner layers of thin high-permeability ($\mu_r = 100000$) material which typically have a lower saturation field (0.9 T) such as Cryoperm. This passive shielding is enhanced by an external copper coil driven with high current to partially deplete the magnetic field in the region of interest. For this design VTT has performed finite element method (FEM) simulations as shown in Figure 4.4.2. Regarding the third location for the experiments below the 4-K plate the stray field is smaller, but still expected to require multilayer shield design.

The approach at RISE was to use a commercial dry cryostat system, *Teslatron* from *Oxford Instruments*, and to modify it to operate both a quantum Hall resistance standard and a Josephson voltage standard in parallel. The cryostat (Figure 4.4.3, left) consists of a vacuum enclosure with a two-stage pulse tube cooler. The first stage cools down to about 50 K and the second stage cools to just below 4 K. A superconducting 12 T magnet at the bottom is cooled to its superconducting state by the second cooling stage. Inside the magnet core is a separate sample space which is further cooled by a helium circulation system down to 1.5 K.

To achieve the integration of a Josephson standard in the same cryostat, a separate enclosure was installed in the insulation vacuum of the cryostat which is cooled by the 4 K plate. Figure 4.4.3 (middle) shows the enclosure. To minimise the thermal load, the upper part of the tube is made from a thin-walled stainless steel tube thermally anchored to the 50 K plate with a group of four copper braids (Figure 4.4.3, left). The bottom of the tube consists of a hollow copper closed tube for cooling the Josephson standard. This is anchored to the 4 K plate with 9 short copper braids and a copper block tightly attached to the upper part (Figure 4.4.3, left). Mechanical vibrations from the pulse tube coolers should be strongly attenuated by the flexible connections.

To provide the needed magnetic shielding, a shield made from Cryoperm (commercial trade name), an alloy with very high permeability at cryogenic temperatures was used. The shield is a cylinder with a closed bottom and 2 mm thick walls. This should be sufficient (see section 4.4.2) since the distance to the magnet is much higher than in the VTT system.

Figure 4.4.3: (left) *The cryostat with the vacuum container and heat shield removed. At the bottom can be seen the superconducting magnet coil.* ***(middle)*** *The Josephson standard enclosure consists of a thin-walled stainless steel tube for thermal isolation and a hollow copper end for cooling the Josephson chip.* ***(right)*** *The enclosure mounted in the cryostat with thermal straps to the 50 K plate (aluminium) and the 4 K plate (copper)*

4.4.2 Operation of the Josephson voltage source

For the VTT approach an optically pulse driven JVS which minimises the heat load to the cryostat is planned. Several proof-of-concept studies have recently been published. Instead of using a high-bandwidth coaxial cable to bring the driving current pulses to the array, an optical fibre illuminating an ultra-fast photodiode is used to produce the required pulse patters.

The Josephson probe for the RISE cryocooler system consists of a chip holder with the Josephson chip (both provided by PTB) glued into it, a waveguide, and a vacuum tight room temperature connection box (Figure 4.4.4). The chip holder is made from copper and it fits snugly into a slot at the bottom of the copper end of the enclosure. Two sections of the waveguide are made from stainless steel in order to minimise the heat transport to the cold end of the probe. Above the middle of the waveguide, between the stainless-steel sections, are two copper braid loops which connect to the inside of the stainless-steel tube, where the 50 K thermal connection is attached on the tube's outside.

Figure 4.4.4*:* ***(left)*** *The Josephson probe is shown upside down. It consists of a connection box at room temperature, a rectangular waveguide with a ribbon cable wrapped around it, and a copper holder for the Josephson chip.* ***(middle)*** *Close-up of the Josephson chip holder provided by PTB. It is made from copper and the Josephson chip (not visible) is firmly glued to the copper for optimum cooling.* ***(right)*** *The room temperature connection box is vacuum*

tight with vacuum compatible connections for current biasing, voltage output, temperature sensor and waveguide (not visible)

The temperature at the probe end reached about 5.7 K during different test runs at RISE. This was enough to observe the Josephson supercurrent (Figure 4.4.5). In order to test the magnetic shielding, the supercurrent was observed while ramping the superconducting magnet in the cryostat up to 10 T. Any magnetic field leaking through the Cryoperm shield should reduce the supercurrent and make it impossible to operate the Josephson standard. In the tests at RISEno effect on the supercurrent could be detected, which convincingly prooves that the shielding is sufficient.

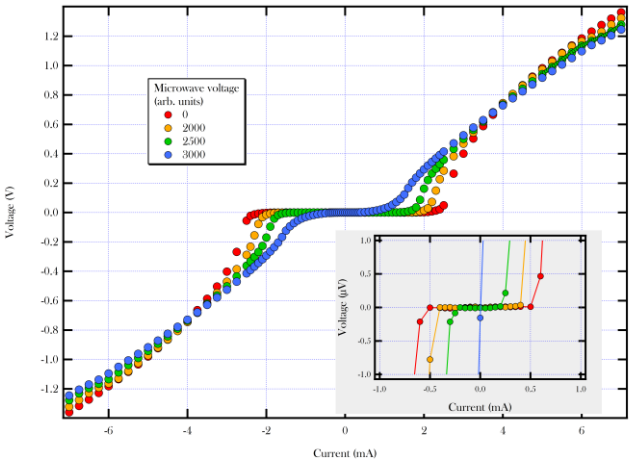

Figure 4.4.5: *Current-voltage characteristics of the Josephson standard with different microwave amplitudes. With increasing microwave levels the supercurrent gradually decreases, until it disappears completely (see inset graph). Ideally there should be a flat Shapiro step at 1.2 V, but there is only a subtle hint of it*

However, the temperature of the Josephson chip was not cold enough. With microwaves on and suitable bias currents, there should be a flat Shapiro step (at 1.2 V with this chip). Presumably the temperature needs to be even lower in order to generate a quantised output voltage with the Josephson standard.

4.4.3 Operation of the graphene quantum Hall resistance device

The sample space in the RISE system is used to operate the quantum Hall standard, which needs a strong magnetic field. Extensive tests of graphene quantum Hall devices have been performed and were very satisfactory. Figure 4.4.6 shows the low noise level of the measurements, in spite of some mechanical vibrations from the pulse tube cooler and helium circulation pump.

The sample space is mechanically disconnected from the rest of the cryostat, except at the heavy stainless steel top plate, therefore vibration levels are strongly attenuated. Thin copper wires were used in the probe for connection to the graphene chip.

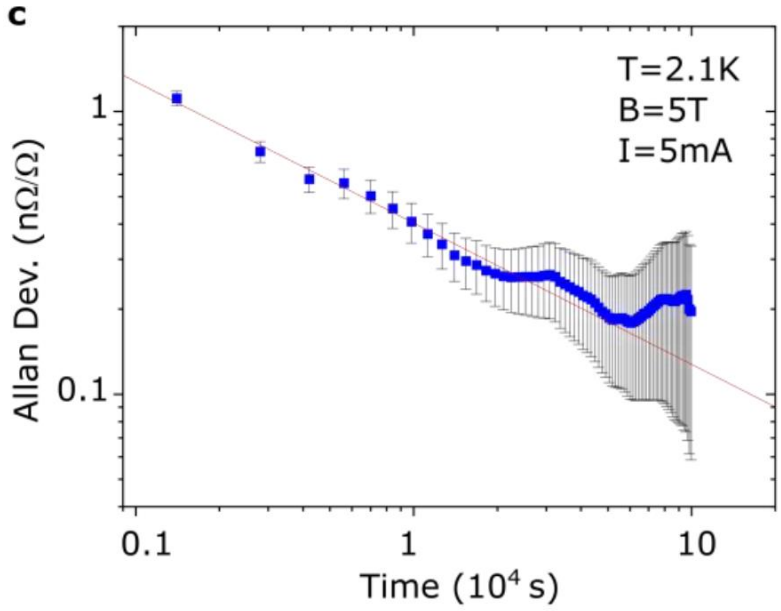

Figure 4.4.6: *Measurement of a quantum Hall standard in the dry cryostat has a low noise level. The Allan deviation is a measure of the noise level and a value below 1 nΩ/Ω is good in this application*

Conclusion

Both systems have had significant progress towards the goal of this project and are close to the final experiment of simultaneous operation of a Josephson voltage standard (with quantised output voltage) and a graphene QHR standard. The prospects for a single cryogenic system serving as the core element of a quantum resistance and impedance standard as well as voltage and current standards in the revised SI are very promising and allow a successful completion of the final experiment. The major challenges for the set up and operation of a single cryogenic system for metrological applications were solved within this project and the related objective was reached. Both VTT and RISE will continue their efforts still after formal termination of the GIQS project.

4.5 Uptake of the technology and measurement infrastructure developed in the project by stakeholders) (Objective 5)

Several actions were made over the course of the project to facilitate the take up of the technology developed in the different work packages.

4.5.1 Connections with the user community

- The project created a large stakeholder committee of more than 40 representatives from nearly 30 organisations worldwide. The organisations are public bodies and universities as well as industry – from small to large enterprises – from graphene manufactures to electronic device suppliers.
- The project website, social media channels (YouTube, LinkedIn, ResearchGate) and a web repository (Zenodo) were created to inform stakeholders and all interested parties.

  https://www.ptb.de/empir2019/giqs/home/

  https://www.linkedin.com/groups/8824119/

  https://www.youtube.com/channel/UCaHuyb8YzrjPnLUz7nSiauA

https://www.researchgate.net/publication/346288018_The_EMPIR_Project_GIQS_Graphene_Impedance_Quantum_Standard

https://zenodo.org/communities/?p=giqs

- Five issues of a periodical newsletter were distributed among the stakeholders and other interested persons. It is also available from the project's webpage.
- An online questionnaire to understand the needs was initiated.

Two major online events dedicated to the project were held including:

- A two-days virtual stakeholder workshop and training with an audience of 60 people worldwide. The project experts shared their experience with a series of lectures and the playing of short videos recorded in their laboratories. The videos are being posted on the social media channels of the project.
- Dozens of presentations at specialised conferences and external events were performed.
- Connections with metrology institutional and technical committees (e.g. the Consultative Committee for Electricity and Magnetism of the Metre Convention) were established.
- The connection to the Stakeholder community will be maintained after the formal end of the project. News regarding the project's topics will still be distributed via the website and social media platforms.

4.5.2 Dissemination of the scientific outcome

The scientific outcome of the project was disseminated towards the scientific community with

- open-source papers, a book chapter and PhD theses and conference proceedings.
- Publication of papers was advertised on the social media channels and the newsletter issues.
- Several videos with details of the fabrication of graphene devices, the operation of impedance bridges, and the realisations of the SI units were produced and distributed.
- Papers on non-specialised literature were published.
- Papers at the Graphene Flagship Conferences were presented.
- To convince the end users that the improvement in the performances of the new technologies are justified by the high investments needed, the project focused not only on ultimate accuracy, but also on the reduction of the instrumental and personnel expenses that are necessary to acquire and operate the instrumental setups proposed to the stakeholders.
- Within the lifetime of the project the interest of the stakeholders continuously raised and uptake actions have already been achieved:

4.5.3 Dissemination of technology and infrastructure

(i) Graphene devices

- The project conclusively demonstrated that the graphene devices developed in the course of the project can reliably be employed for the SI realisation of the resistance and capacitance units ohm and farad.
- The simplified operation of calibration infrastructure by using the new graphene-based resistance standards is presented in PTB's Quantum Technology Centre which offers measurement opportunities to industry and calibration centres.
- The interest of several National Metrology Institutes and of the Bureau International of Poids and Mesures (BIPM) was raised, which experimented with a PTB device for the realisation of resistance under relaxed experimental conditions.
- The experimentation was successful and publicly recognised on the BIPM website with the news given in Figure 4.5.1.

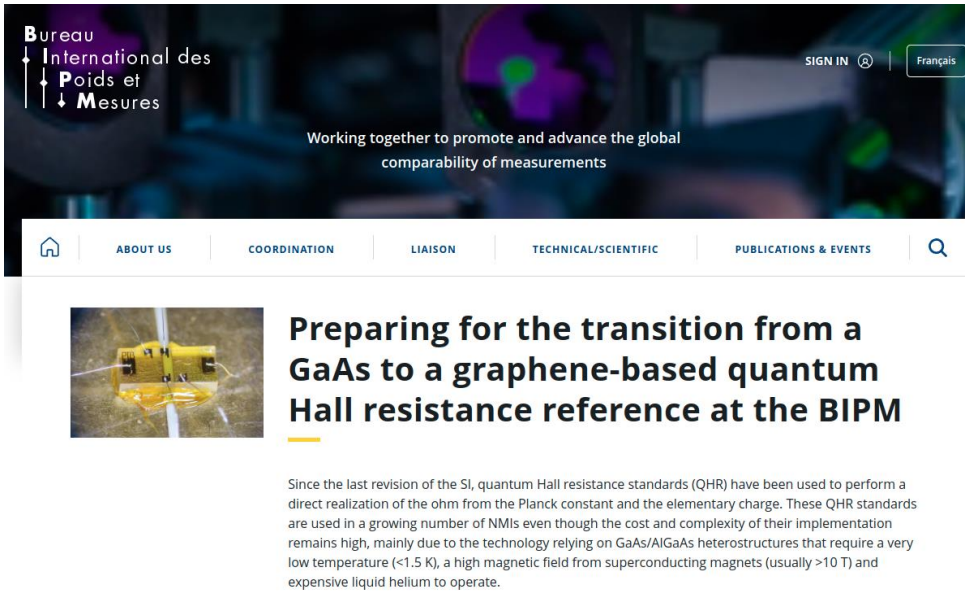

Figure 4.5.1. *Screenshot of the BIPM website acknowledging the use of the GIQS graphene devices for the realisation of the ohm under relaxed experimental conditions*

(ii) Impedance bridges

- Digital impedance bridges are presently recognised as the main road towards the realisation of impedance units and scales from the quantum Hall effect, as acknowledged also by the main international conference on electromagnetic metrology, the Conference on Precision Electromagnetic Measurements, which in the 2022 edition established the topic “Quantum Impedance Bridges”.
- A requirement plan has been drawn up for the knowledge transfer of advanced impedance bridge systems from experienced NMIs to those with less experience.
- Early uptake of project results by knowledge transfer of project results to smaller NMIs has been realised by a new cooperation between the National Institute of Metrology Thailand (NIMT) and PTB. An agreement was signed for training of scientists and acquisition of a dual Josephson waveform synthesizer for multipurpose applications, including a Josephson impedance bridge.

5 Impact

To promote the uptake of the progress in the field of impedance metrology and epitaxial graphene fabrication technology generated in this project, as well as to share insights generated throughout the project, the results were shared broadly with scientific and metrology end-users.

Twelve papers in international peer-reviewed journals, a book chapter and two PhD theses were published and submitted, respectively. 33 presentations were held at conferences, including those associated to the Graphene Flagship, the Conference on Precision Electromagnetic Measurements, the International Metrology Conference, the IMEKO TC-4 conferences, and the URSI General Conference. Information on the GIQS activities were spread to regulatory bodies. In the past years the EURAMET committee TC-EM (Electricity and Magnetism) was regularly informed about the progress of the GIQS project at the annual contact person meeting as well as at the 23rd TCEM meeting of the Asian Pacific Metrology Programme (APMP). Technical committees of GULFMET, COOMET and SIM were also kept informed. The CCEM has adopted one of the Newsletter issues as a working document.

19 lab training activities were carried out for scientists from the consortium and for external audiences, among them 8 presentations at university seminars. The consortium disseminated project results in many other ways, e.g. PhD theses and articles in trade journals.

Five newsletter issues which summarise the goals and results of the project were produced and distributed to stakeholders. To inform stakeholders, the scientific community and interested end users about news from the project in the short term, four online platforms were created. Next to the project's homepage, GIQS groups exist on LinkedIn and ResearchGate. 15 tutorial videos on the latest research results in the field of graphene fabrication for quantum metrology and impedance measurements using the developed bridges are available from the GIQS YouTube channel.

To learn more about the needs and expectations of the stakeholders the consortium has proactively launched a survey among potential stakeholders. In a subsequent joint stakeholder meeting the consortium presented the results in the work packages and a discussion about further activities was started. In Winter 2020 a dedicated workshop for stakeholders and collaborators was organised online.

Impact on industrial and other user communities

This project established a new primary standard of impedance. At present, industrial and other user communities rely on a long chain of calibrations, originating at the BIPM or few large NMIs, and extending over smaller NMIs, and/or commercial calibration service providers to eventually reach the end user. This lengthy chain has been shortened with a simpler, cheaper and easier to operate primary standard. The impact on industrial and other end users will gain its full thrust after an initial post-project phase when the knowledge and know-how created in this project has been taken up by instrumentation companies and converted into marketable solutions e.g a digital impedance bridge based on conventional electronics. The early impact will be on industrial instrumentation manufacturers and large-scale calibration service providers, which will be able to use the enhanced calibration quality enabled by the new primary impedance quantum standard to provide scientifically sound services with improved performance, reliability and cost efficiency.

Impact on the metrology and scientific communities

At present many small NMIs obtain traceability for their national resistance and capacitance standards from other NMIs or from BIPM due to the high acquisition and operational costs of primary quantum Hall systems. For example, from 2013 – 2017, BIPM issued 159 certificates for resistance and 127 for capacitance for 36 NMIs. Eighteen of them were from Europe. Therefore, at the NMI level, one of the major impacts of the project will be to provide a direct and user-friendly realisation of impedance units in the "revised SI" at the "point of calibration", thereby relaxing the NMIs' dependence on BIPM, and releasing BIPM's resources for more important research tasks.

To create early impact in the scientific communities, research papers have been published in high impact peer-reviewed journals. Dissemination workshops will also be organised for different target groups.

As explained in the draft mise en pratique for the ampere and other electrical units in the revised SI, the unit farad can be realised by comparing the quantised Hall resistance to the impedance of the unknown capacitance using, for example, a quadrature bridge. Development of digital solutions, e.g. digital conventional bridges, for such a primary unit realisation will be one of the main impacts of this project. The graphene-based quantum Hall resistance (QHR) device is also valuable in the realisation of other electrical units of the revised SI, such as the unit ampere that can be realised *"by using Ohm's law, the unit relation A = V/Ω, and using practical realisations of the SI derived units volt V and ohm Ω, based on the Josephson and quantum Hall effects, respectively"*. For those NMIs who decide to implement the new impedance quantum standard, such direct access to the primary capacitance realisation will enable them to claim improved CMCs in this field.

The BIPM has publicly recognised the relevance of the approach proposed by the GIQS project by performing dc electrical metrology experiments with graphene devices developed within the project.

Impact on relevant standards

This project will create impact as an impedance calibration system based on a quantum standard is now available. How this new primary quantum standard, and especially its possible use outside of authorised NMIs, will impact the international measurement system and written standards need to be discussed by the relevant bodies of the international measurement system. However, this project has actively contributed to key European and international committees (e.g. Consultative Committee for Electricity and Magnetism (CCEM)) to spread the required information and knowledge.

In this context, the most important regulatory document is EN ISO/IEC 17025, “General requirements for the competence of testing and calibration laboratories”, which defines in general terms the technical requirements for good practice calibrations in section 6.5 (2017). Furthermore, calibration is an important and recurring subject in the EC directive MID 2004/22/IEC on measuring instruments. National laws and directives in the EU member states concerning the units of measurements and how they are to be implemented are relevant law whose simpler, better, and more cost-effective compliance will be targeted by the developments in this project.

Longer-term economic, social and environmental impacts

Achieving the objectives of this project will respond to the need for a shorter traceability chain to quantum impedance standards by using the huge metrological potential of graphene. It will also preserve and strengthen Europe’s lead in the metrological applications of the QHE in graphene and in digital impedance metrology.

The European calibration services market was estimated to be worth $1.55 billion in 2018, with more than 40 % of the total being for electrical calibrations, which include instrument calibrations for radiation dosimetry, medical diagnostics and treatment, smoke detectors, devices for environmental monitoring, semiconductor wafer characterisation, etc. Even a relatively small improvement in the accuracy for the end users, as a result of the shortened calibration chain targeted in this project, will generate a very significant amount of economic benefit for the EU. In the technology sector, where the benefit-to-cost ratio of electrical measurements is amongst the highest, the development of new types of devices, sensors, and measurement methods with faster speed, higher sensitivity, and lower energy consumption, will become possible.

The long-term environmental impact of this project will be indirect, yet strong; many measurement techniques, be they environmental, medical or scientific, make use of transducing elements based on capacitance. Improving the traceability to capacitance will improve the sensitivity and reproducibility of such measurement techniques, leading in turn to improved data quality which will lead to several benefits: more efficient engines, a reduction in exhaust gases, the measurement of polluting particulates, and to an improvement in electrical impedance spectroscopy for geophysics, to name only some. The political benefit of the research will be that a high-end primary standard will become attainable for almost every metrology or calibration laboratory. Proliferation of primary quantum standards is one of the key aims of international metrology and it allows all countries to interact on an equal basis.

6 List of publications

[1] J. Park, W.-S. Kim, and D.-H. Chae, Realization of 5h/e2 with graphene quantum Hall resistance array, Appl. Phys. Lett. 116, 093102 (2020). https://doi.org/10.1063/1.5139965

[2] D. Momeni Pakdehi, P. Schädlich, T. T. Nhung Nguyen, A. A. Zakharov, S. Wundrack, E. Najafidehaghani, F. Speck, K. Pierz, T. Seyller, C. Tegenkamp, and H. W. Schumacher, Silicon Carbide Stacking-Order-Induced Doping Variation in Epitaxial Graphene, Adv. Funct. Mater. 30, 2004695 (2020). https://doi.org/10.1002/adfm.202004695

[3] M. Marzano, M. Ortolano, V. D’Elia, A. Müller, and L. Callegaro, A fully digital bridge towards the realization of the farad from the quantum Hall effect, Metrologia 58, 015002 (2021). https://doi.org/10.1088/1681-7575/abba86

[4] S. Bauer, R. Behr, R. E. Elmquist, M. Götz, J. Herick, O. Kieler, M. Kruskopf, J. Lee, L. Palafox, Y. Pimsut, and J. Schurr, A Four-Terminal-Pair Josephson Impedance Bridge Combined with a Graphene Quantized Hall Resistance, Meas. Sci. Technol. 32,065007 (2021), https://doi.org/10.1088/1361-6501/abcff3

[5] M. Kruskopf, S. Bauer, Y. Pimsut, A. Chatterjee, D. K. Patel, A. F. Rigosi, R. E. Elmquist, K. Pierz, E. Pesel, M. Götz, and J. Schurr, Graphene quantum Hall effect devices for ac and dc electrical metrology, IEEE Transactions on Electron Devices 68, 3672 (2021). https://doi.org/10.1109/TED.2021.3082809

[6] M. Marzano, N. T. Mai Tran, V. D'Elia, D. Serazio, E. Enrico, M. Ortolano, K. Pierz, J. Kučera, L. Callegaro, Design and development of a coaxial cryogenic probe for precision measurements of the quantum Hall

effect in the AC regime, ACTA IMEKO 10, 24 – 29 (2021). http://dx.doi.org/10.21014/acta_imeko.v10i2.925

[7] D.-H. Chae, M. Kruskopf, J. Kucera, J. Park, N. T. Mai Tran, D. B. Kim, K. Pierz, M. Götz, Y. Yin, P. Svoboda, P. Chrobok, F. Couëdo, and F. Schopfer, Investigation of the stability of graphene devices for quantum resistance metrology at direct and alternating current, Meas. Sci. Technol. 33, 065012 (2022). https://doi.org/10.1088/1361-6501/ac4a1a

[8] M. Marzano, Novel devices and methods for quantum resistance and impedance metrology, PhD thesis, 2020, Politecnico di Torino, https://iris.polito.it/handle/11583/2779393#.YKvCzKgzaUk

[9] Momeni Pakdehi, Davood., Optimization of Epitaxial Graphene Growth for Quantum Metrology, PhD thesis, 2020, Gottfried Wilhelm Leibniz Universität Hannover, Germany, https://doi.org/10.15488/10201

This list is also available here: https://www.euramet.org/repository/research-publications-repository-link/